https://doi.org/10.5194/acp-2019-769
Preprint. Discussion started: 7 October 2019

Atmospheric Chemistry and Physics Discussions

Measurements to determine mixing state of black carbon emitted from the 2017/2018 California wildfires and urban Los Angeles

Joseph Ko[1], Trevor Krasowsky[1,*], George Ban-Weiss[1]

[1]Department of Civil and Environmental Engineering, University of Southern California, Los Angeles, 90089, USA
[*]now at: SpaceX, 1 Rocket Rd, Hawthorne, CA 90250 USA

Correspondence to: George Ban-Weiss (banweiss@usc.edu)

Abstract. The effects of atmospheric black carbon (BC) on climate and public health have been well established, but large uncertainties remain regarding the extent of BC's impacts at different temporal and spatial scales. These uncertainties are largely due to BC's heterogeneous nature in terms of its spatiotemporal distribution, mixing state, and coating properties. Here, we seek to further understand the mixing state evolution of BC emitted from various sources and aged over different timescales using field measurements in the Los Angeles region. We measured refractory black carbon (rBC) with a single-particle soot photometer (SP2) on Catalina Island, California (~70 km southwest of downtown Los Angeles) during three different time periods. During the first campaign (September 2017), westerly winds dominated and thus the sampling location was upwind of the dominant regional sources of BC (i.e., urban emissions from the Los Angeles basin). In the second and third campaigns (December 2017, November 2018), atypical wind conditions caused measured rBC to include important contributions from large wildfires in California and urban emission from the Los Angeles basin. We observed a larger number fraction of thickly coated particles (f_{BC}) and increased coating thickness (CT_{BC}) during the first campaign (~0.27 and ~36 nm, respectively), and during portions of the third campaign when we suspect that rBC was transported long-range from the Camp Fire in Northern California (~0.35 and ~52 nm, respectively), compared to other time periods. In contrast, during periods when we suspect that measured rBC was dominated by Southern California fires or urban emissions, both f_{BC} and CT_{BC} were significantly lower, with a mean f_{BC} of ~0.03 and median CT_{BC} ranging from ~0 to 10 nm. From our rBC measurements and meteorological analyses, we conclude that an aging timescale on the order of ~hours is not long enough for rBC to become thickly coated under the range of sources sampled and atmospheric conditions during this campaign. On average, we found that measured rBC had to age more than a day to become thickly-coated. Aging timescales for developing thick coatings were found to be longer in this study relative to a number of previous observational studies conducted with an SP2, suggesting that rBC aging is heavily impacted by regional atmospheric context.

https://doi.org/10.5194/acp-2019-769
Preprint. Discussion started: 7 October 2019

Atmospheric Chemistry and Physics Discussions

1 Introduction

Atmospheric black carbon (BC) is a carbonaceous aerosol that can result from the incomplete combustion of carbon-containing fuels. Major energy-related sources of BC include vehicular combustion, power plants, residential fuel-use, and industrial processes. Biomass burning, which can be either anthropogenic or natural, is another significant BC source. BC is a pollutant of particular interest for two main reasons: (1) it strongly absorbs solar radiation, which results in atmospheric warming (Ramanathan and Carmichael, 2008), and (2) it is associated with increased risk of cardiopulmonary morbidity and mortality (World Health Organization, 2012). Regarding its effect on climate, BC is widely considered to be the second strongest contributor to climate warming, after carbon dioxide (Bond et al., 2013). Although it has been established that BC is a strong radiative forcing agent in Earth's atmosphere, there remains considerable uncertainty about the extent to which BC affects Earth's radiative budget, from regional to global scale (IPCC, 2013; Bond et al., 2013).

Since the lifetime of BC is relatively short (~days to weeks), the spatiotemporal distribution of BC is highly heterogeneous, making it difficult to quantify (Krasowsky et al., 2018). The quantification of where and when BC is emitted around the world is also a challenging task that causes significant uncertainties (Bond et al., 2013). In addition to the difficulties that come with tracking the emissions and distribution of BC, there are complex physical and chemical processes that govern the transformation of BC in the atmosphere, which ultimately impact its climate and health effects. BC is emitted mostly as an "external" mixture, physically separated from other aerosol species. Although BC is likely coated to some extent by non-refractory organic and non-organic compounds at the point of emissions (Johnson et al., 2005), "fresh BC" is generally conceptually considered uncoated. As fresh BC is transported in the atmosphere, it obtains inorganic and organic coatings from either gaseous pollutants that condense onto the BC, oxidation reactions on the BC surface, or the coalescence of other aerosol species onto the BC (He et al., 2015). Aged BC that has acquired coatings is referred to as *internally mixed BC* (Bond et al., 2006; Schwarz et al., 2008). In general, the *mixing state* of BC describes how much BC is either externally or internally mixed within a broader aerosol population (Bond et al., 2013).

The evolution of rBC mixing state as the BC ages in the atmosphere is crucial to understand for two reasons. First, it has been shown that non-refractory coatings on BC can enhance its absorption efficacy, implying that internally mixed BC with thick coatings can have stronger warming potential in the atmosphere compared to uncoated or thinly-coated BC (Moteki and Kondo., 2007; Wang et al., 2014). Second, coatings on BC can alter the aerosol's hygroscopicity and effectively shorten its lifetime by increasing the probability of wet deposition (McMeeking et al., 2011; Zhang et al., 2015). In short, freshly emitted BC particles are generally hydrophobic, but coatings acquired during the aging process can make BC-containing particles hydrophilic, and therefore, more susceptible to wet deposition. Thus, uncertainties in the evolution of rBC mixing state directly translate to uncertainties regarding BC's impact on Earth's climate due to both the radiative impact per particle mass and spatiotemporal variation of atmospheric BC loading.

https://doi.org/10.5194/acp-2019-769
Preprint. Discussion started: 7 October 2019

Atmospheric Chemistry and Physics Discussions

Although there have been a number of laboratory experiments (Wang et al., 2018; He et al., 2015; Slowik et al., 2007; Knox et al., 2009) and field campaigns (Krasowsky et al., 2018; Metcalf et al., 2012; Cappa et al., 2012; Schwarz et al., 2008) studying rBC mixing state, there is considerable variability in results. For example, field studies in China suggest that the mass absorption cross-section (MAC) of BC that has aged for more than a few hours should be enhanced by a factor of ~2 (Wang et al., 2014), while other studies in California reported an absorption enhancement factor of ~1.06 and ~1.03 (Cappa et al. 2012; Krasowsky et al., 2016). Preceding these studies, Bond et al. (2006) suggested an enhancement factor of ~1.5 based on a review of laboratory and field studies. The wide range of reported values is not surprising given that rBC mixing state is expected to be influenced by a variety of spatiotemporal factors such as source type, season, and regional atmospheric composition (Krasowsky et al., 2018). In other words, BC aged in different places, at different times, may have significantly varying mixing states, resulting in a wide range of absorption and hygroscopicity enhancements in the real world.

Quantifying rBC mixing state is challenging because it requires single-particle analysis (Bond et al., 2006). There are two main methods to measure rBC mixing state: (1) microscopy (Johnson et al., 2005), and (2) real-time, in-situ measurements (Hughes et al., 2000). In our study, we quantify rBC mixing state by taking real-time, in-situ measurements with a single particle soot photometer (SP2). The SP2 uses laser-induced incandescence to measure refractory black carbon (rBC) mass per particle, which can be used to directly compute the mass concentration, number concentration, and mass size distribution, and indirectly compute the number size distribution (Stephens et al., 2003). The SP2 can also measure the internal mixing state of rBC using one of two different methods. In the lag-time method, each sensed rBC-containing particle is deemed as either *thinly-coated* or *thickly-coated* using the measured time difference between the peak of the particle's incandescence and scattering signal (Moteki and Kondo, 2007). In the leading-edge-only (LEO) method, the actual coating thickness for rBC-containing particles can be explicitly quantified (Gao et al., 2007). Further detail regarding these two methods can be found in section 2.3 and 2.4. In this study, we used both methods to quantify the rBC mixing state.

In this study, we measured rBC with an SP2 on Catalina Island, California (~70 km southwest of Los Angeles) during three different time periods, with the goal of observing how rBC loading and mixing state varied as a function of source type and source-to-receptor timescale. During the first campaign (September 2017), westerly winds dominated and thus the sampling location was upwind of the dominant regional sources of rBC (i.e., urban emissions from the Los Angeles basin). We suspect measurements during this period to represent well-aged particles, some of which might have originated from wildfires in Oregon and Northern California. In contrast, the second and third campaigns (December 2017, November 2018) were dominated by northerly-to-easterly "Santa Ana conditions", which advected fresh and aged rBC-containing particles from both biomass burning emissions and urban emissions. Several significant wildfires were active in the Southern and Northern California regions throughout the second and third campaigns. In particular, the Thomas Fire, which was active in Southern

https://doi.org/10.5194/acp-2019-769
Preprint. Discussion started: 7 October 2019

Atmospheric Chemistry and Physics Discussions

California during the second campaign, was the second largest wildfire in modern California history. The Camp Fire, which was active in Northern California during the third campaign, was the 16th largest fire in terms of burn area size, and was also considered the deadliest and most destructive wildfire in modern California history. Table 1 lists the two most significant wildfires for each campaign period that we suspect had some impact on our rBC measurements, along with the total burn area and time period of non-containment for each fire. Mass and number concentrations of rBC-containing particles, rBC size distributions, the number fraction of thickly coated rBC-containing particles (i.e., using the lag-time method), and absolute coating thickness values (i.e., using the LEO method) are reported. We then evaluate how the rBC loading, size distribution, and mixing state relate to the meteorology and major sources at the time of measurements in order to further understand the microphysical transformation of BC as it ages in the atmosphere. While a few past studies have investigated the mixing state of rBC in the Los Angeles region using the SP2 (Metcalf et al., 2012; Cappa et al. 2012; Krasowsky et al. 2018), this study is the first to use fixed ground-based measurements off the coast of Los Angeles to focus on how (a) wildfire source-to-receptor travel time, and (b) wildfire versus urban emissions, influence rBC mixing state.

Table 1. Major wildfires that were active during the three campaigns. Only the two biggest fires from each campaign (in terms of burn area in acres) are listed in the table below. Note that there were numerous other smaller fires that were active during the three campaigns, but not listed in this table.

Campaign	Wildfire name	Location	Area (km^2)	Start date	Containment date
First (September 2017)	Chetco Bar Fire	Rogue River–Siskiyou National Forest, Oregon	773	12 July, 2017	2 November, 2017
	Eclipse Complex	Siskiyou, California	318	15 August, 2017	29 November, 2017
Second (December 2017)	Thomas Fire	Ventura and Santa Barbara, California	1,140	4 December, 2017	12 January, 2018
	Creek Fire	Los Angeles, California	63	5 December, 2017	9 January, 2018
Third (November 2018)	Camp Fire	Butte, California	620	8 November, 2018	25 November, 2018
	Woolsey Fire	Ventura, California	392	8 November, 2018	22 November, 2018

https://doi.org/10.5194/acp-2019-769
Preprint. Discussion started: 7 October 2019

Atmospheric Chemistry and Physics Discussions

2 Methods

2.1 Measurement location and time periods

All measurements reported in this study were conducted at the USC Wrigley Institute for Environmental Studies on Catalina Island (~33°26'41.68"N, 118°28'55.98"W). Catalina Island is located approximately 70 km (43.5 miles) southwest of downtown Los Angeles. Figure 1 shows the location of the sampling site relative to the Los Angeles metropolitan area. The three campaigns were conducted from 7 to 14 September 2017, 20 to 22 December 2017, and 12 to 18 November 2018.

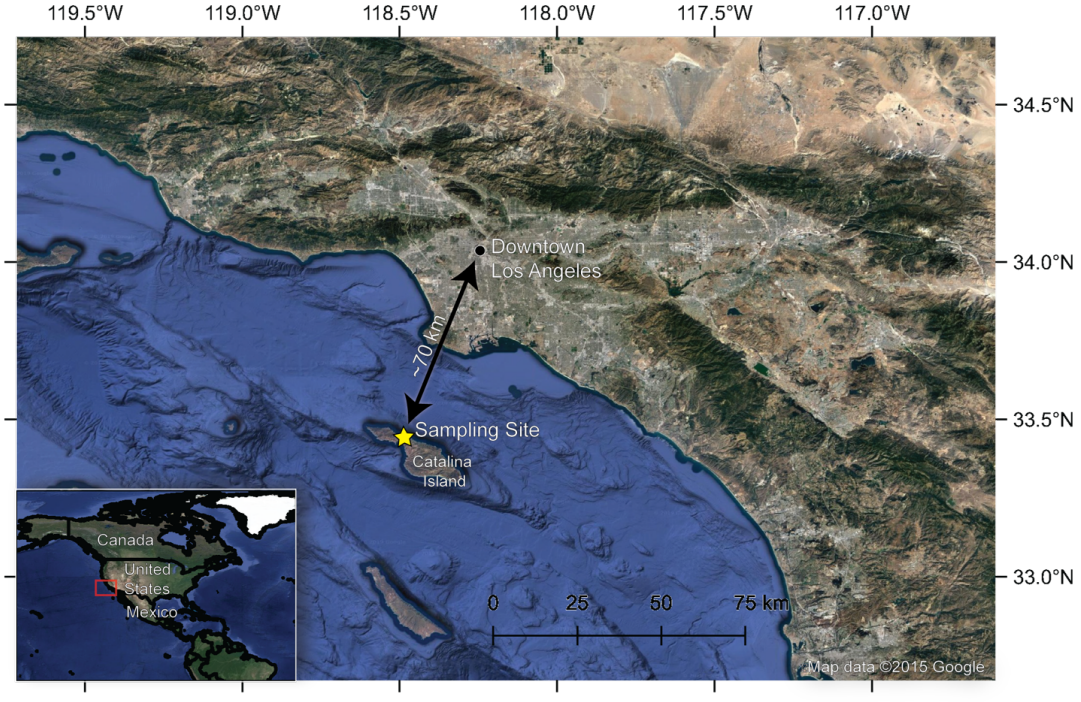

Figure 1. Overview map showing the location of the sampling site with respect to the Greater Los Angeles (LA) area.

2.2 Instrumentation

An SP2 (Droplet Measurement Technologies, Boulder, CO) was used to quantify the physical characteristics of rBC-containing particles for all three campaigns. In short, the SP2 uses laser-induced incandescence to quantify rBC mass on a particle-by-particle basis. The SP2 uses a continuous Nd:YAG laser (λ = 1064 nm) that is oriented perpendicular to the flow

https://doi.org/10.5194/acp-2019-769
Preprint. Discussion started: 7 October 2019

Atmospheric Chemistry and Physics Discussions

of air containing rBC-containing particles. As each particle passes through the intra-cavity laser, any coating on the rBC particle vaporizes while the core incandesces and emits thermal radiation. The scattered and thermally emitted radiation is measured by optical sensors and converted to signals that can then be used to obtain information about the mass and mixing state of the sampled rBC-containing particles. The SP2 has detection limits from ~0.5 to 50 fg rBC per particle. Further details regarding the governing principles and operation of the SP2 can be found in numerous publications (Stephens et al., 2003; Schwarz et al., 2006; Gao et al., 2007; Moteki and Kondo, 2007; Laborde et al., 2012; Dahlkötter et al., 2014; Krasowsky et al., 2016).

The inlet of the SP2 was positioned on the roof of a three-story research building at the Wrigley Institute as shown in Figure S1. The height of the inlet was approximately 15 meters above ground level. A fine mesh was secured to the tip of the inlet to prevent clogging by small insects, and a small plastic cone was also attached to block any potential precipitation from entering the inlet. The inlet tube was fed in through a window of a secure laboratory room on the top floor of the building where the SP2 was housed for the duration of sampling. The SP2 ran continuously for the duration of the three sampling periods. Desiccant used to remove moisture from the sample air was replaced on a daily basis, and the data during these replacement periods were subsequently removed during the data analysis.

2.3 Auxiliary data

Model simulations and publicly available auxiliary datasets were used to supplement our SP2 measurements.

The National Oceanic and Atmospheric Administration's (NOAA) Hybrid Single-Particle Lagrangian Integrated Trajectory (HYSPLIT) model (Stein et al., 2015) was the primary tool used to identify dominant emissions sources. The HYSPLIT back-trajectories were also used to estimate the age range of measured rBC-containing particles and the path of the air masses carrying these particles. The HYSPLIT trajectory model requires the user to specify the following input parameters: meteorological database, starting point of the back-trajectory, height of source location, run time, and the vertical motion method. A height of 15 meters above ground level was chosen to approximately represent the height of the SP2 inlet positioned on the roof of the laboratory facility. For the first campaign (September 2017), the Global Data Assimilation System (GDAS) meteorology database with 1-degree resolution (~110 km for 1-degree latitude and ~85 km for 1-degree longitude) was selected, and one-week back-trajectories were simulated for every day of the first campaign. For the second and third campaigns (December 2017, November 2018), the High-Resolution Rapid Refresh (HRRR) meteorology database with a 3-km resolution was selected, and 72-hour back-trajectories were simulated starting on every hour. The GDAS database was selected for the first campaign simulations because a 1-degree resolution was sufficient to show that the measured air masses were generally coming from the west. In contrast, the HRRR database was used for the second and third

https://doi.org/10.5194/acp-2019-769
Preprint. Discussion started: 7 October 2019


Atmospheric Chemistry and Physics Discussions

campaigns because a finer resolution helped determine the sources that contributed to measured rBC. The default vertical motion method was selected for all back-trajectory simulations.

Data from local weather stations were used to identify the meteorological regimes during all three campaigns, and to supplement the HYSPLIT back-trajectories used for source characterization. Hourly weather data from Los Angeles International Airport (LAX), Long Beach Airport, Avalon (Catalina Island), Santa Barbara, and Oxnard, during September 2017, December 2017, and November 2018, were obtained using the NOAA National Center for Environmental Information online data tool (https://www.ncdc.noaa.gov/cdo-web/datatools/lcd, last access: 26 August 2019). Five-minute weather data at the same weather stations and time periods were obtained from the Iowa Environmental Mesonet website (https://mesonet.agron.iastate.edu, last access: 26 August 2019; Todey et al.,2002). Wind data from the USC Wrigley Institute on Catalina Island were also examined when available (7 to 13 September 2017) on the Weather Underground website (https://www.wunderground.com/weather/us/ca/catalina, last access: 26 August 2019), though these data are not validated by NOAA. Data from Santa Barbara, Oxnard, and USC Wrigley Institute were assessed to support conclusions made in this study, but are not directly presented in any of the analyses here.

In addition to meteorological data, weather information from local news reports, NASA satellite imagery, and global aerosol model data were used in conjunction to explain the variability in rBC concentrations and mixing state during the sampling campaigns. Local weather news reports between 20 December and 22 December 2017 were used to obtain information about the active fires in Southern California and the dominant wind conditions for each day in the second campaign (December 2017) (CBS Los Angeles, 2017a, 2017b, 2017c, 2017d, 2017e, 2017f). There were generally two local weather reports retrievable per day: one in the early morning and one later on in the evening. The information from these reports was used to get a holistic picture of the local fire and weather conditions at the time of sampling. Data from the California Department of Forestry and Fire Protection (https://www.fire.ca.gov/incidents/, last access: 26 August 2019) was also used to verify basic spatial and temporal information about significant fires occurring during sampling periods. The local weather reports were used to cross-validate wildfire timelines, but they are not directly presented here.

NASA satellite imagery and data were accessed through NASA's Worldview online application (https://worldview.earthdata.nasa.gov/, last access: 26 August 2019), which provides public access to NASA's Earth Observing System Data and Information System (EOSDIS). Moderate Resolution Imaging Spectroradiometer (MODIS) images taken from two satellites (Aqua and Terra) were examined for all sampling days. MODIS images were used to identify visible plumes of aerosols, particularly those from large wildfires. The general movement of air masses was also assessed from the visible movement of large-scale clouds from these satellite images. In addition to the MODIS images, aerosol index, aerosol optical depth (AOD), and fires and thermal anomalies data products were examined to supplement the source identification process. For aerosol index, the OMAERUV (Torres, 2006) and OMPS_NPP_NMTO3_L2 (Jaross,

https://doi.org/10.5194/acp-2019-769
Preprint. Discussion started: 7 October 2019


Atmospheric Chemistry and Physics Discussions

190 2017) products were used. For AOD, the MYD04_3K MODIS/Aqua and MYD04_3K MODIS/Terra products were used (Levy et al., 2013). For fires and thermal anomalies, the VNP14IMGTDL_NRT (Schroeder et al., 2014) and MCD14DL (Justice et al., 2002) products were used. Examples of NASA data products used for source identification analysis can be found in the Supplement.

195 An open-source online visualization tool (earth.nullschool.net, last access: 26 August 2019) was used to visually assess the European Centre for Medium-Range Weather Forecasts (ECMWF) Copernicus Atmosphere Monitoring Service (CAMS) model output data (Beccario, 2019; https://atmosphere.copernicus.eu/, last access: 26 August 2019). The CAMS model provides "near-real-time" forecasts of global atmospheric composition on a daily basis. Specifically, the $PM_{2.5}$ concentration output data from CAMS were examined using earth.nullschool.net. The CAMS output visualizations were particularly
200 helpful for understanding where certain sources were located and when they were likely affecting our measurements. The concentration gradients of $PM_{2.5}$ were examined on the visualization tool on an hourly interval for every day of active sampling in order to supplement the HYSPLIT analysis and confirm the contribution of certain emission sources. Access to the CAMS visualizations for the three campaigns can be found in the Supplement and Video Supplement.

2.4 Estimation of source-to-receptor timescale

205 Characteristic timescales of transport between the sampling site and nearest source(s) were estimated based on the HYSPLIT trajectories simulated for source identification. The approximate source-to-receptor timescale characterizations by HYSPLIT were cross-validated with approximate calculations of transport time performed with representative length scales between sources and the sampling site, and the average wind speeds during the time periods of interest. Further details regarding the calculations of the timescale characterizations are in section S1 of the Supplement. Although we cannot fully capture the
210 intricacies of particle aging timescales with our estimates, they are meant to be conservative approximations based on available meteorological data. These estimated source-to-receptor timescales were used to help categorize different LEO periods by source(s) (see Figure 6), and also used in our discussion of how rBC mixing state evolves with particle aging (see Section 3.6).

2.5 Time series filtering

215 rBC mass and number concentrations during the first campaign (September 2017) showed anomalous spikes likely due to unexpected local sources. In an effort to obtain representative background concentrations, we filtered these spikes by removing values above a threshold of 0.08 μg m^{-3} and 40 cm^{-3} for mass and number concentrations, respectively. Figure S2 in the Supplement shows the time series for the first campaign before and after removal of spikes. Figure S3 in the Supplement shows the median rBC concentration for the first campaign as a function of the cut-off threshold value. Median
220 rBC mass and number concentrations appeared to asymptote at cut-off values of approximately 0.08 μg m^{-3} and 40 cm^{-3},

https://doi.org/10.5194/acp-2019-769
Preprint. Discussion started: 7 October 2019


Atmospheric Chemistry and Physics Discussions

suggesting that the median rBC concentration values become insensitive to the choice of cut-off threshold above these values.

2.6 Lag-time method

The mixing state of rBC was examined using two different methods. The first method used to characterize mixing state is called the lag-time method. This method categorizes each rBC particle as either "thickly-coated" or "thinly-coated" based on a measured time delay (i.e., "lag-time") between the scattering and incandescence signal peaks. This method has been previously described and used in various studies (Moteki and Kondo, 2007; McMeeking et al., 2011; Metcalf et al., 2012; Wang et al., 2014; Krasowsky et al., 2016; Krasowsky et al., 2018). In short, as a coated rBC-containing particle passes through the SP2 laser, the sensors will detect a scattering signal as the coating vaporizes. Shortly after, there will be a peak in the incandescence signal as the rBC core heats up and emits thermal radiation. A probability density function of the lag-time values often results in a bimodal distribution. Based on the data for a particular campaign, a lag-time cut-off is chosen between the two peaks of the bimodal distribution to bin each rBC particle as either thinly or thickly coated. The fraction of rBC particles that are thickly-coated (f_{BC}) is then determined based on this categorization. For our study, a lag-time cut-off of 2 μs was chosen to quantify whether an rBC-containing particle was thickly-coated. As discussed previously by Krasowsky et al. (2018), the lag-time method is inherently susceptible to biases since f_{BC} can depend on the selection of the lag-time cut-off value. For example, Krasowsky et al. selected a cut-off value of 1 μs for a near-highway SP2 campaign in the Los Angeles Basin, which is significantly different than the value of 2 μs used in this study and others. There remains an unresolved issue of maintaining consistency between different studies utilizing the lag-time method, while simultaneously representing the unique mixing state characterization of each measured rBC population; the definition of "thickly-coated" likely varies by the aerosol population sampled and thus is not necessarily comparable from one study to the next.

2.7 Leading-edge-only (LEO) method

BC mixing state was also characterized using the LEO method. In brief, this method reconstructs a Gaussian scattering function from the leading edge of the scattering signal for each rBC-containing particle. The width and location of the reconstructed Gaussian scattering function is determined by a two-element avalanche photodiode. Assuming a core-shell morphology, the rBC coating thickness is subsequently calculated from the reconstructed scattering signal and the incandescence signal (Gao et al., 2007). The Paul Scherrer Institute's single-particle soot photometer toolkit version 4.100b (developed by Martin Gysel et al.) was used to perform the LEO method in Igor Pro version 7.09. For our study, the LEO "fast-fit" method was used with the first three points of the leading edge, and particles analyzed were restricted to those with rBC core diameters between 200 and 250 nm. Although the SP2 has been reported to accurately measure the volume equivalent diameter (VED) of scattering particles down to ~170 nm, a more conservative lower threshold of 200 nm was

https://doi.org/10.5194/acp-2019-769
Preprint. Discussion started: 7 October 2019

Atmospheric Chemistry and Physics Discussions

used for our study to reduce instrument noise at smaller VED values near the detection limit, as done in our previous study (Krasowsky et al., 2018).

3 Results and discussion

3.1 Source identification and meteorology

In this section, we summarize the dominant pollutant sources and wind patterns for each of the three campaigns. For all three campaigns, we used HYSPLIT back-trajectories, CAMS model data, and NASA data products (i.e., satellite imagery, aerosol index products, and AOD products) in conjunction to identify the most likely sources of measured rBC-containing particles. For the first campaign (September 2017), the Oregon wildfires were identified as probable sources of measured rBC. Furthermore, we also identified long-range transport from East Asia and ship/aviation emissions as potential sources contributing to measured rBC. Overall, we expect measured rBC during the first campaign to be aged. For the second campaign (December 2017), fresh urban emissions from the Los Angeles basin and biomass burning emissions from the Thomas Fire in Santa Barbara and Ventura County (along with other smaller Southern California fires) were the main sources identified by our analysis. For our third campaign (November 2018), fresh urban emissions from the Los Angeles basin and fresh biomass burning emission from the Woolsey Fire in Ventura (along with other smaller Southern California fires) were the main sources identified for approximately the first four days of the campaign. For approximately the last two days of the third campaign, we suspect that the Camp Fire in Northern California (along with other smaller fires in Northern and Central California) had significant contributions to measured rBC. Figure 2 displays the percentage of wind coming from different directions, for each campaign, at three different weather station locations (public data provided by NOAA, see section 2.3). Furthermore, Figure 3 shows HYSPLIT back-trajectories simulated for each of the three campaigns and further highlights in detail, the differences in wind conditions between the three campaigns. These figures clearly show the distinct meteorological regimes of each campaign. A more detailed description of the source identification process can be found in section S1 of the Supplement.

https://doi.org/10.5194/acp-2019-769
Preprint. Discussion started: 7 October 2019

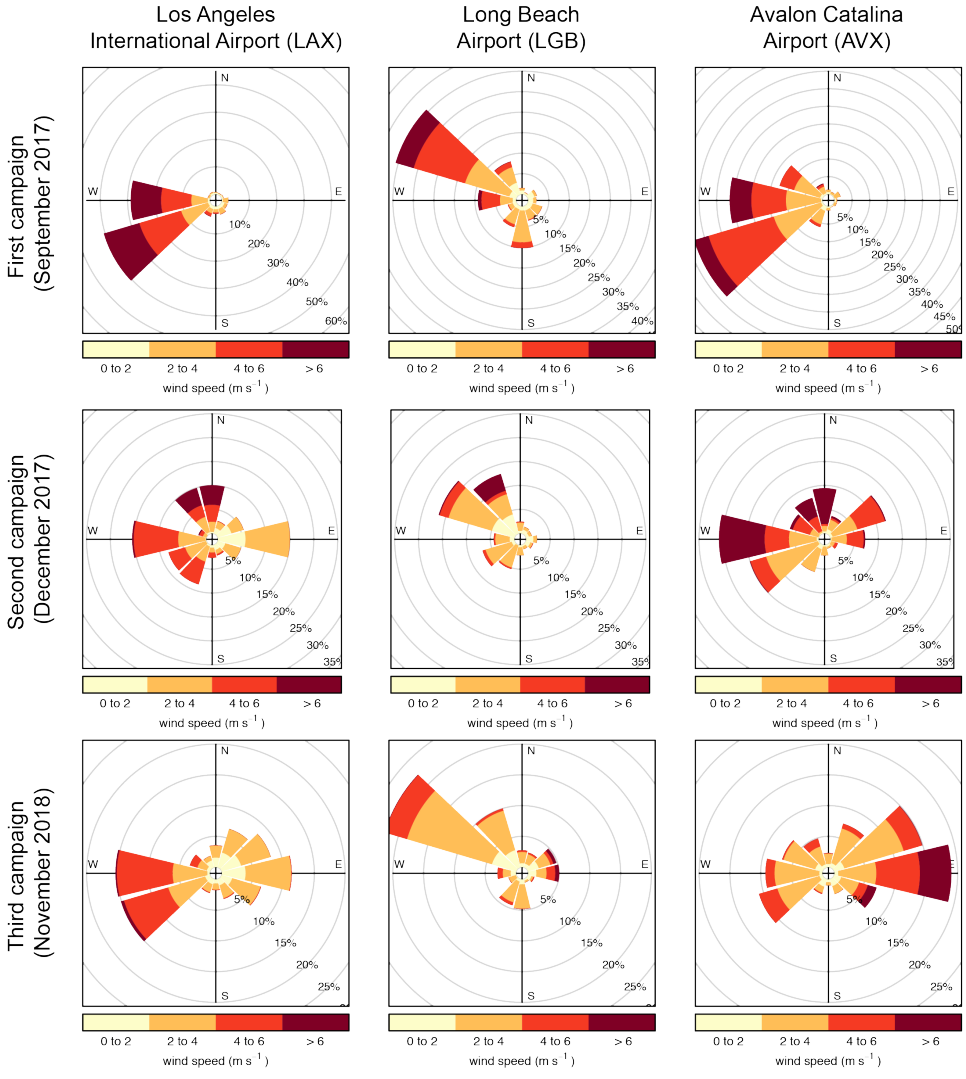

Figure 2. Wind roses for the September 2017 (first row), December 2017 (second row), and November 2018 (third row) sampling periods. Wind roses are based on five-minute ASOS airport data from LAX (first column), LGB (second column), and AVX (third column), provided by NOAA.

https://doi.org/10.5194/acp-2019-769
Preprint. Discussion started: 7 October 2019

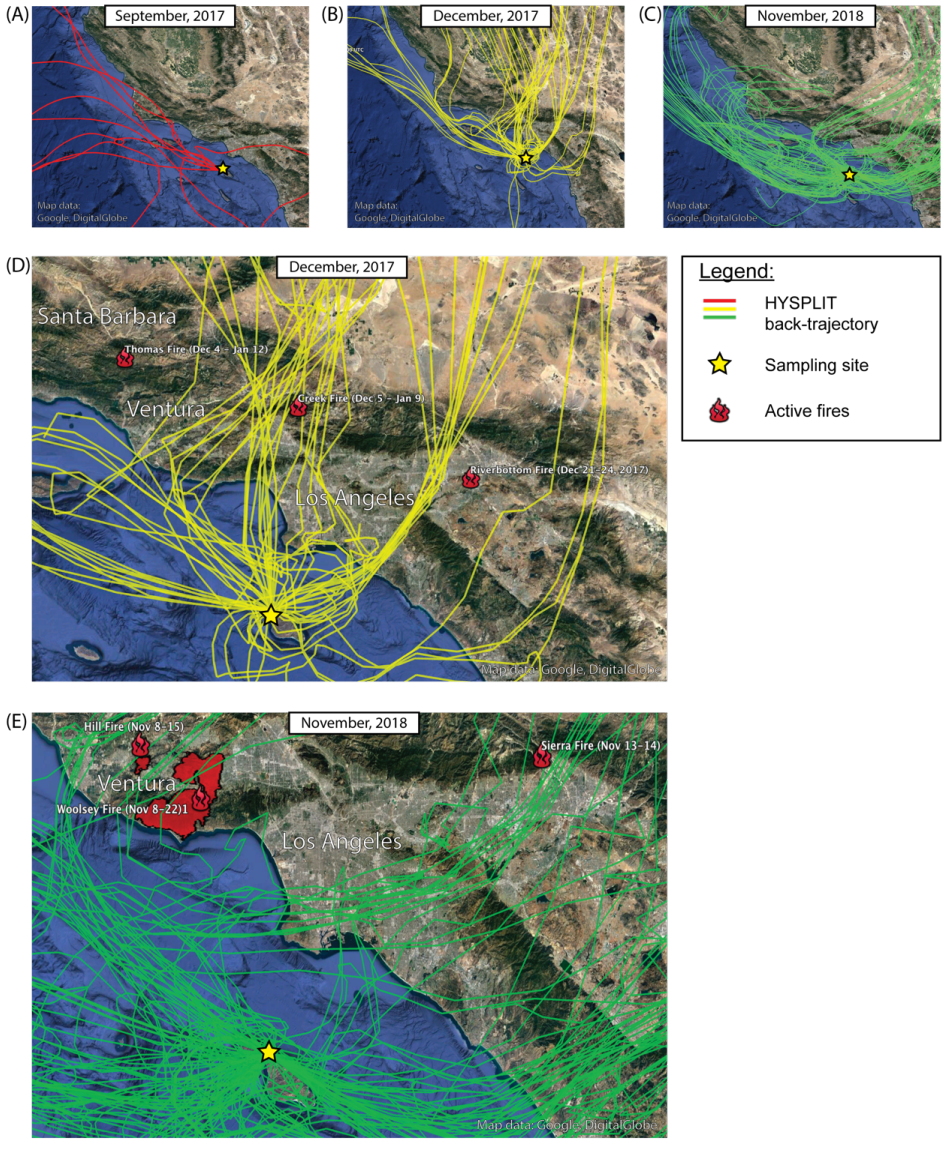

Figure 3. HYSPLIT back-trajectories for all three campaigns. The star denotes the start location of each back-trajectory, i.e., the sampling location. The trajectories for the first period (September 2017) (i.e., panel a) represent week-long back-trajectories for each day of the campaign. The trajectories for the (b) second (December 2017) and (c) third (November 2018) periods represent 72-hour back-trajectories for each hour of the campaign. Panels (d) and (e) show more zoomed-in maps of the second and third campaign back-trajectories along with active Southern California fires shown. © Google. Digital Globe.

https://doi.org/10.5194/acp-2019-769
Preprint. Discussion started: 7 October 2019

Atmospheric Chemistry and Physics Discussions

3.2 rBC mass and number concentration

Figure 4 shows time series for rBC mass and number concentrations and f_{BC} for all three measurement campaigns. The mean mass and number concentration (±standard deviation) for the first campaign (September 2017) was 0.04 (±0.01) μg m^{-3} and 20 (±7) cm^{-3}, respectively. For the second campaign (December 2017), the corresponding mean concentrations were 0.1 (±0.1) μg m^{-3} and 63 (±74) cm^{-3}, with concentrations reaching as high as 0.6 μg m^{-3} and 381 cm^{-3}. Likewise, for the third campaign (November 2018), the corresponding mean concentrations were 0.15 (±0.1) μg m^{-3} and 80.2 (±54.5) cm^{-3}. The range of observed rBC concentrations is larger for the second and third campaigns compared to the first campaign, and there are distinct prolonged peaks in concentrations that can be observed during these times; in comparison, the first campaign shows relatively stable concentrations.

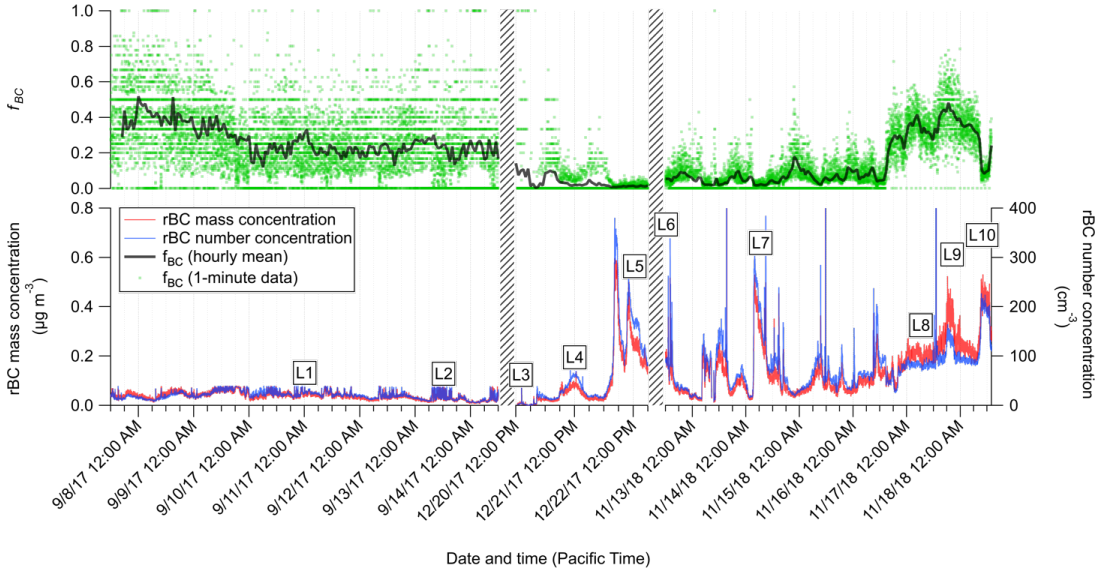

Figure 4. Time series of rBC concentrations and the fraction of rBC particles that are thickly coated (f_{BC}) for all three measurement campaigns. The boxed annotations (i.e., L1 to L10) refer to specific LEO periods, which are further described in Section 3.4. In the upper panel, green dots represent one-minute means while the black curve shows hourly means. The lower panel shows one-minute means.

Given the remote location of the sampling site and the consistent westerly winds during the first campaign (September 2017), the observed rBC concentrations establish an appropriate baseline for ambient conditions away from the broader urban plume in the Los Angeles basin. On the other hand, the concentrations during the second and third campaigns

https://doi.org/10.5194/acp-2019-769
Preprint. Discussion started: 7 October 2019

Atmospheric Chemistry and Physics Discussions

(December 2017, November 2018) were more variable and the mean concentrations were higher than the mean concentration for the first campaign due to periods of northerly-to-easterly winds driven by Santa Ana wind conditions as described in section 3.1. Figure 5 shows rBC mass and number concentrations along with wind speed and direction during the second campaign. Wind direction was directly related to elevated concentrations for all three peaks shown. Peak P1 is clearly preceded by a prolonged period of northerly winds. Similarly, Peaks P2 and P3 are preceded by periods of easterly winds. An analogous plot for the third campaign is shown in Figure S9, but the relationship between wind direction measured at LAX and the rBC concentration is not clearly discernible since long distance biomass emissions were impacting the measurements in addition to local sources near the LA basin. The impacts of different sources on measurements during the third campaign are described in detail in section S2 of the Supplement.

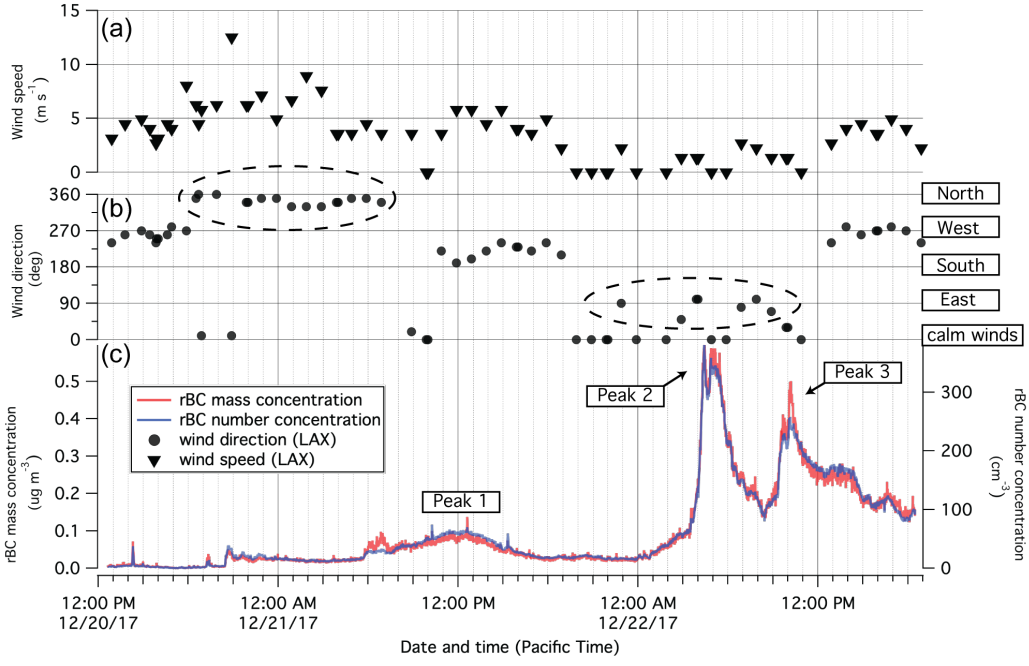

Figure 5. Meteorological variables and rBC concentrations during the second campaign (December 2017). Panel (a) shows wind speed and (b) shows wind direction measured by a NOAA weather station located at Los Angeles International Airport (LAX). Panel (c) shows rBC mass and number concentrations and identifies three peaks of interest. The two dashed ovals in panel (b) highlight periods of northerly and easterly winds, which occur ~0.5-1 days before each of the three peaks, suggesting that the elevated rBC concentrations included important contributions from the local Thomas Fire and Los Angeles basin (i.e., biomass burning and urban emissions).

On average, the concentrations for the first campaign (September 2017) were approximately an order of magnitude lower than the average concentration of ~0.14 μg m^{-3} observed by Krasowsky et al. (2018) near the outskirts of the LA Basin, in

https://doi.org/10.5194/acp-2019-769
Preprint. Discussion started: 7 October 2019

Atmospheric Chemistry and Physics Discussions

Redlands. Concentrations during the most polluted time periods in our measurements (i.e. parts of the second and third campaigns) were comparable to recently measured concentrations in the Los Angeles basin (Krasowsky et al., 2018) but at least one to two orders of magnitude lower than average concentrations found in other heavily polluted cities around the world. Mass concentration values of ~0.9 μg m^{-3}, ~0.5 to 2.5 μg m^{-3}, ~0.9 to 1.74 μg m^{-3}, and ~0.6 μg m^{-3} were measured with an SP2 in Paris, Mexico City, London, and Houston, respectively (Laborde et al., 2013; Baumgardner et al., 2007; Liu et al., 2014; Schwarz et al., 2008). In urban areas of China, an average mass concentration of ~9.9 μg m^{-3} was reported for a polluted period in Xi'an (Wang et al., 2014).

3.3 Lag-time analysis: number fraction of thickly-coated rBC-containing particles

Figure 4 shows both one-minute and one-hour averages for f_{BC} over the course of all three campaigns. On average, f_{BC} was larger during the first campaign (September 2017) than during the second and third campaigns (December 2017, November 2018). The mean values (±standard deviation) of f_{BC} were 0.27 (±0.19), 0.03 (±0.09), and 0.14 (±0.15) for the first, second, and third campaigns, respectively. This implies that about one-quarter of the rBC-containing particles that were measured in the first campaign had sufficient time in the atmosphere to become aged with thick coatings, while most of the rBC measured in the second campaign was fresh. The rBC from the third campaign exhibited mostly thinly-coated rBC for approximately the first four days of the campaign and an increased f_{BC} for approximately the last two days of the campaign.

Compared to past studies in the Los Angeles region, the average f_{BC} for the first campaign (September 2017) (0.27) is close to the lower end of values from past aircraft measurements (0.29) (Metcalf et al., 2012) and the upper end of previous ground-based measurements (0.21) (Krasowsky et al., 2016). In contrast, the mean value of f_{BC} for the second campaign (December 2017) is almost an order of magnitude lower than the average for the first campaign. There are some periods with slightly elevated f_{BC} during the second campaign, but the overall trend suggests that most of the rBC-containing particles in this period are thinly-coated or essentially uncoated. The Santa Ana wind conditions during the second campaign advected fresh (a) urban emissions from the Los Angeles basin, and/or (b) biomass burning emissions from active fires in Southern California, as discussed in section 3.1.

The third campaign (November 2018) is unique in that both "fresh" and "aged" rBC-containing aerosols from biomass burning were measured. As shown in Figure 4, there is a distinct period of relatively higher f_{BC} and rBC concentrations starting at approximately noon on 16 November 2018 and lasting through the end of the campaign on 18 November 2018. This is the only period from all three measurement campaigns where we observed *both* an elevated rBC mass/number loading and f_{BC}. In section 3.1, we identified the Camp Fire to be the predominant source during this time period within the third campaign. This implies that rBC-containing particles from the Camp Fire were contributing to the elevated rBC mass/number loadings and had sufficient time in the atmosphere to acquire thick coatings and thus increase f_{BC}.

https://doi.org/10.5194/acp-2019-769
Preprint. Discussion started: 7 October 2019

Atmospheric Chemistry and Physics Discussions

3.4 Leading-edge-only (LEO) fit analysis: rBC coating thickness

To further examine the mixing state of rBC-containing particles, the leading-edge-only (LEO) fit method was used to quantify rBC coating thickness (CT_{BC}) during various time periods of interest. Two time periods from the September campaign, three time periods from the December campaign, and five time periods from the November campaign were selected to represent a diverse range of meteorological conditions, emission sources, and age of aerosols. Table 2 lists the ten LEO-fit periods, and their median and mean CT_{BC}. The LEO-fit periods are also annotated on the rBC concentration time series (see Figure 4) to show when they occurred in the context of all three campaigns. The median CT_{BC} for the LEO periods ranged from –0.3 to 55.9 nm. L6 had the lowest median CT_{BC} (–0.3 nm), while L9 had the highest median CT_{BC} (55.9 nm).

Table 2. Details of the ten different LEO time periods.

LEO Time Period	Date/Time (PST)	Period Length (mins)	Total number of rBC particles analyzed[a]	Median coating thickness (nm)	Mean coating thickness (nm)
L1	11 Sep. 2017, 12:00-1:01am	61	453	36.4	44.2
L2	13 Sep. 2017, 11:59-12:58pm	59	464	23.9	28.4
L3	20 Dec. 2017, 12:59-2:00pm	61	158	42	44.1
L4	21 Dec. 2017, 12:29-1:00pm	31	601	10.9	13.4
L5	22 Dec. 2017, 9:59-10:15am	16	1,143	10.7	13.3
L6	12 Nov. 2018, 12:00-1:00pm	60	1,748	-0.3	5.6
L7	14 Nov. 2018, 5:00-6:00am	60	1,886	8.4	10.9
L8	17 Nov. 2018, 5:00-6:00am	60	945	49.2	58.6
L9	17 Nov. 2018, 7:00-8:00pm	60	983	55.9	68.6
L10	18 Nov. 2018, 10:00-11:00am	60	1,122	31.3	40.7

[a] LEO coating thickness calculations were performed only for rBC particles with core sizes between 200 and 250 nm.

Figure 6 illustrates the CT_{BC} distributions and statistics of each LEO period. L1 and L2 were from the first campaign (September 2017). L1 is representative of ambient background rBC-containing particles from the first campaign. A period that did not exhibit any anomalously large rBC mass concentration values was chosen so that contributions from possible nearby sources would not skew the average CT_{BC}. On the other hand, L2 intentionally spans a period with many anomalously high rBC mass concentration values. Although these anomalous values were removed from the concentration time series discussed previously in section 2.4, the values were *not* removed for the LEO analysis of L2 in order to examine the relationship between CT_{BC} and possible nearby emissions. As hypothesized, the rBC-containing particles from L2 were generally more thinly coated than those from L1. The median CT_{BC} from L2 was 12.5 nm *thinner* than that for L1, which

https://doi.org/10.5194/acp-2019-769
Preprint. Discussion started: 7 October 2019

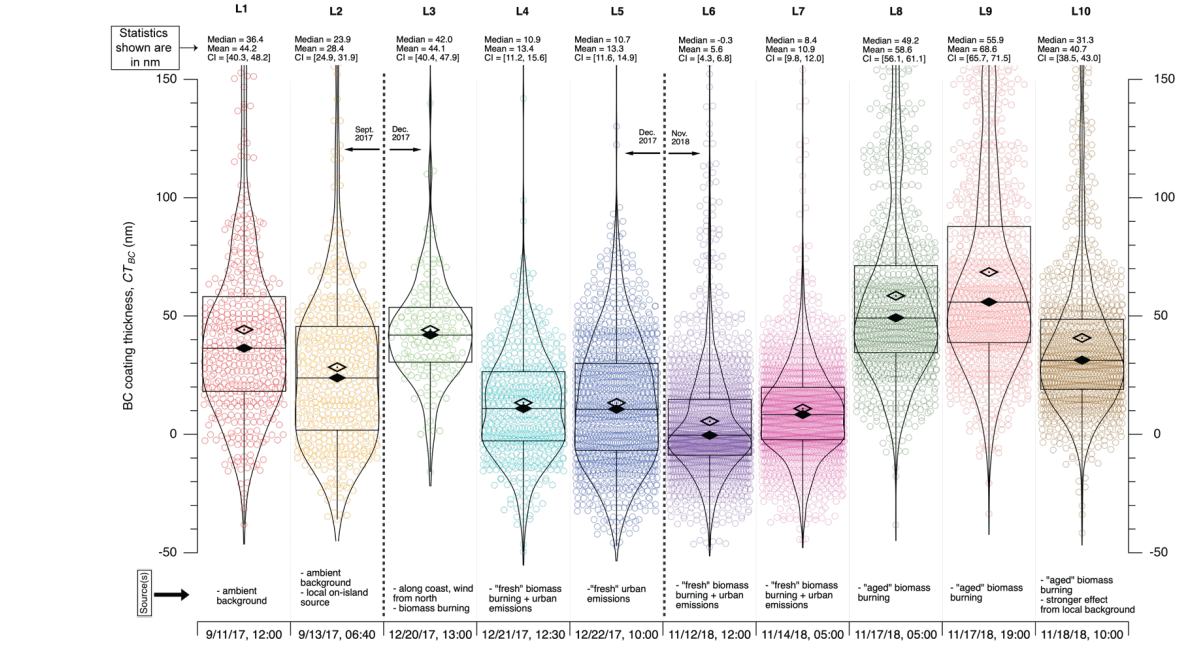

Figure 6. Violin plots that show the distribution of rBC coating thickness values calculated for each LEO time period, L1 through L10. Each circle marker in the plot represents a particle analyzed by the LEO analysis and the curves for each "violin" shape represents the normalized probability density function of the coating thickness for each LEO period. The violin shapes are simply a result of mirroring each distribution along a vertical axis. Box-and-whiskers plots are also overlaid to show the quartiles (25th, 50th, and 75th percentiles) of the coating thickness distributions. The 95% confidence intervals (CI) based on Student's t-distribution are shown above each violin plot to demonstrate when the mean coating thickness values are statistically distinguishable from one another. The mean and median coating thicknesses are also indicated above each violin plot, and a brief description of sources for each LEO period is annotated below each violin plot.

https://doi.org/10.5194/acp-2019-769
Preprint. Discussion started: 7 October 2019


Atmospheric Chemistry and Physics Discussions

corroborates our hypothesis that the anomalously high mass concentration values in the first campaign included contributions from nearby sources.

L3 through L5 are time periods from the second campaign (December 2017). L3 represents a period near the start of the second campaign (December 2017). The predominant wind direction during L3 was westerly, with an average wind speed of ~4.5 m s^{-1}. HYSPLIT back-trajectories and CAMS data show that L3 likely included important contributions from the Thomas Fire in Santa Barbara and Ventura County. The $PM_{2.5}$ concentration gradient from CAMS was examined over time to track the movement of plumes that influenced the measurements during this time period. A few days prior to the start of the second campaign, the Thomas Fire emitted a large aerosol plume westward over the Pacific Ocean. From visually tracking $PM_{2.5}$ concentration gradients, it appears that a large-scale, clockwise, atmospheric circulation brought aerosols from the Thomas Fire to Catalina Island around the time of L3 (see video 2 of Video Supplement). The average concentration during L3 was about an order of magnitude lower than the average concentration for the September campaign. This could be partially attributed to the fact that L3 was around 1 to 2 pm, when the planetary boundary layer would be expected to increase in height, causing pollutants concentrations to decrease due to dilution. The median CT_{BC} for L3 was 42 nm, which is slightly thicker than the median CT_{BC} found for L1, which is representative of the ambient background conditions. The slightly larger CT_{BC} for L3 might reflect the fact that mixing state is sensitive to the source of emissions. A number of previous studies have suggested that rBC from biomass burning emissions are generally more thickly coated (Sahu et al., 2012; Schwarz et al. 2008; Dahlkötter et al., 2014). In this case, we have evidence to suspect that a larger fraction of measured rBC during L3 came from the local Thomas Fire, while L1 represents a mix of influences, including, but not limited to, aged biomass burning aerosols.

L4 through L7 represent periods of time when the Los Angeles basin and Santa Barbara/Ventura counties (which includes both biomass burning and urban emissions) were identified as major sources. The HYSPLIT back-trajectories for these periods pass near several significant local fires in the Southern California region. We also expect urban emissions (i.e., mostly vehicular emissions) to be contributing to the measurements during these periods, when trajectories are generally traversing through urban areas of Southern California. Overall, these LEO periods exhibit the lowest median CT_{BC}. The relationship between aging time and CT_{BC}, especially for these urban emissions influenced periods, is discussed further in section 3.6.

L8, L9, and L10 are the unique LEO periods from the third campaign (November 2018) with elevated f_{BC} (discussed in the previous section). We also observed the highest median CT_{BC} values during these periods. L8 and L9 were both periods of stable elevated f_{BC} and rBC concentrations. We have strong evidence to support that the sampled particles include important contributions from aged rBC from the Northern California fires, particularly the Camp Fire (see section S2 in Supplement). The relatively high CT_{BC} values in L8 and L9 (compared to other LEO periods) further support our claim that rBC-

https://doi.org/10.5194/acp-2019-769
Preprint. Discussion started: 7 October 2019


Atmospheric Chemistry and Physics Discussions

containing particles from Northern California fires were dominating our measurements during this time. L10 has a median CT_{BC} that is ~20 nm smaller than the median values in L8 and L9. This reduction in the median CT_{BC} is also reflected in the decrease of the f_{BC} values near the end of the campaign. Meteorological data, MODIS satellite images, and CAMS data during this time period suggest that sources from the Southern California (and possibly Central Valley) region contributed more to measurements during L10 than they did during L8 and L9, explaining the lower CT_{BC} and higher overall concentrations. Wind speeds were lower on average for L10 compared to L8 and L9. The mean wind speed for L10 at LAX, based on 5-minute NOAA data, was ~1.3 m s^{-1}, while the mean wind speeds for L8 and L9 were ~2.1 m s^{-1} and 1.6 m s^{-1}, respectively. There was also a general shift of wind direction from westerly to north-easterly, approximately a half day before L10 (see figure S9 in Supplement). MODIS satellite imagery and CAMS data also confirm that local to regional sources were likely impacting the measurements more during this period (see video 3 and 4 of Video Supplement), compared to L8 and L9. The stagnant meteorology, in addition to local to regional sources of emissions from the Los Angeles basin and Southern California more broadly, likely explain the reduction in CT_{BC} and the near doubling of the rBC concentration level.

3.5 rBC core size distributions

The number- and mass-based size distributions for rBC cores were assessed for periods L1 to L10. Similar to past studies, rBC core mass equivalent diameters between 70 and 450 nm are reported (Gao et al., 2007; Moteki and Kondo, 2007; Dahlkötter et al., 2014; Krasowsky et al., 2018). Figure 7 shows both log-normal fits of the rBC core size distributions and measured rBC core diameters for three LEO periods (L1, L5, and L10); we investigated these three LEO periods to assess whether log-normal fits adequately represent the actual rBC size distributions before presenting log-normal fits for all LEO periods. Previous studies have shown that rBC core size distributions in nature are generally log-normal in the accumulation mode (Metcalf et al., 2012). Figure 7 shows that log-normal fits adequately capture the measured size distributions, though we cannot rule out the possibility of another rBC mode outside the detection limits of the SP2.

https://doi.org/10.5194/acp-2019-769
Preprint. Discussion started: 7 October 2019

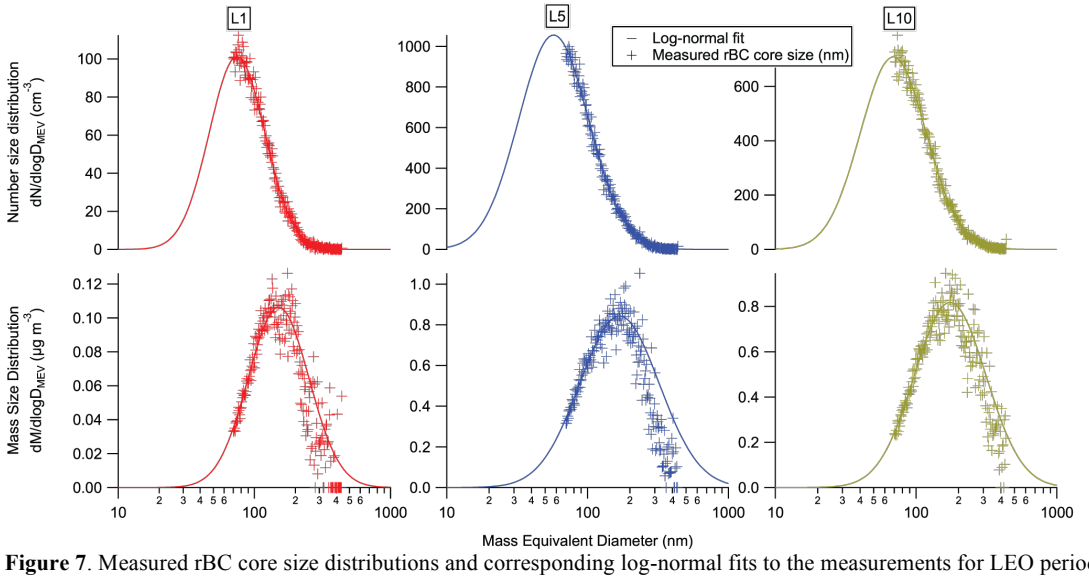

Figure 7. Measured rBC core size distributions and corresponding log-normal fits to the measurements for LEO periods L1, L5, and L10.

Figure 8 shows the median rBC core diameter based on the log-normal fits for each LEO period. There is variability in the median core diameters of both the mass-based and number-based size distributions. Looking specifically at the mass size distribution, the median diameter ranges between 112 nm (L4) and 171 nm (L5, L10). A study by Laborde et al. (2013) discusses the relationship between rBC core diameter and air mass type. According to Laborde et al., an average rBC core diameter of ~100 nm was observed for fresh urban emissions, while diameters of ~200 nm were observed for "continental air masses," which would be expected to be include a larger contribution of aged rBC. The mass size distributions from our LEO periods do not strictly adhere to a positive correlation between aging time and average rBC core diameter as reported by Laborde et al. (2013). In fact, sometimes we observe the opposite relationship. For example, as discussed in the previous section, L5 includes important contributions from freshly emitted rBC, but the mass median diameter is the largest out of all LEO periods (171 nm). Moteki et al. (2012) found negative correlation between aging timescale and rBC core size due to the fractal morphology of the rBC collapsing into a spherical morphology. This mechanism is in direct contrast to the coagulation mechanism described by Laborde et al. (2013), which would serve to increase the mass median rBC core diameter.

https://doi.org/10.5194/acp-2019-769
Preprint. Discussion started: 7 October 2019

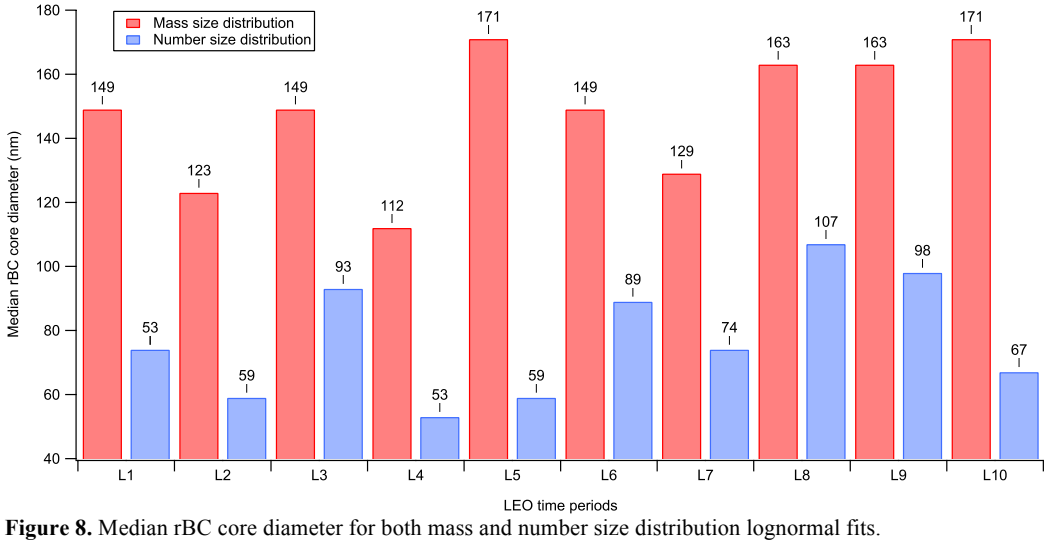

Figure 8. Median rBC core diameter for both mass and number size distribution lognormal fits.

In our study, we observed a mix of rBC core diameters for different periods. For example, L8 and L9 exhibit higher mass median diameters than L4, L6, and L7. We assert that rBC measured during L8 and L9 are more aged than for L4, L6, and L7. As mentioned previously, L5 is inconsistent with the pattern of higher mass median diameter with greater contributions of aged particles. As seen in Figure S10, we see a moderate positive correlation ($R^2 = 0.36$) between median CT_{BC} and the median number-based diameter for rBC. This is consistent with the coagulation mechanism increasing core size with increasing age, as suggested by previous studies (Krasowsky et al., 2018; Laborde et al., 2013; Shiraiwa et al., 2008). In other words, since CT_{BC} generally increases with atmospheric aging, the positive correlation between CT_{BC} and number-based diameter found in this study supports previous suggestions that rBC core sizes increase with atmospheric aging. Additionally, we observe that changes in the mass median diameter are not consistent with the changes in number median diameter, although the figure is not presented here. Although previous studies, like Laborde et al. (2013), have focused on the mass median diameter, our results suggest that the number median diameter could be a more useful metric when correlating core diameters to mixing state metrics since the SP2 measures characteristics of individual rBC particles on a number basis and the CT_{BC} is calculated for each measured particle.

Source type (e.g., urban versus biomass emissions, and different types of fuels burned) can also play a significant role in determining rBC core size (Sahu et al., 2012; Pan et al., 2017; Laborde et al., 2013; Moteki et al., 2012; Metcalf et al. 2012; Wang et al. 2018). Past studies suggest that rBC cores from biomass burning emissions are larger. For example, Metcalf et al. (2012) reported a mass median diameter of ~122 nm for rBC from urban emissions in Los Angeles, while Sahu et al. (2012) reported a mass median diameter of ~190 nm for rBC from biomass burning emissions in various regions around

https://doi.org/10.5194/acp-2019-769
Preprint. Discussion started: 7 October 2019


Atmospheric Chemistry and Physics Discussions

California. Our measurements are in general agreement with previous studies. The mass median diameter of rBC cores measured during periods of strong biomass burning influence (L8-L10) are larger than those calculated for other LEO periods, with the exception of L5 (see Figure 8). This provides further confirmation that rBC core size is influenced by the source of emissions.

3.6 Particle age and rBC mixing state

Table 3 lists the range of estimated "source-to-receptor" timescales for rBC-containing particles measured during LEO time periods L1 to L10. For the first campaign (September 2017), source identification analysis suggests that the measured rBC-containing particles were likely from aged biomass burning emissions and other unidentified sources of aged rBC-containing particles. The fact that all regional emissions were downwind of the sampling site during the first campaign suggests that measured rBC included negligible contributions from fresh emissions from the Los Angeles basin. There were no active wildfires in the Southern California region at the time of the first campaign, but there were significant wildfires in the Pacific Northwest and the northern tip of California (near the California-Oregon border) around the time of measurements, as discussed in section 3.1. We suggest that measured rBC included contributions from these wildfires (see section 3.1), though we make no attempt to quantitatively determining the relative contribution from these wildfires to our measurements.

For the second campaign (December 2017), there was a more diverse range of source types and locations. This was expected, based on the more variable meteorology with respect to the first campaign (September 2017), especially the presence of the less common Santa Ana winds. Fresh urban and biomass emissions influenced air masses (L4 and L5) contained particles with a characteristic age ranging from ~3-12 hours, with an associated median CT_{BC} of ~11 nm. In contrast, L3 had vastly longer aging timescale (~days to week), and an associated median CT_{BC} that was approximately four times higher than that of L4 and L5. The concentrations during L3 were also comparable to the average concentration of the first campaign, which further supports that fresh urban emission sources from the Los Angeles basin were not contributing to the aerosols being measured during the L3 period. The difference in CT_{BC} between periods within the same campaign highlights the relationship between aging timescale and CT_{BC}.

By comparing periods L4-L7 and L8-L9, we estimate a conservative minimum aging timescale for rBC particles to acquire significant coatings. For L4-L7, we observed relatively low values of CT_{BC} and f_{BC}, corresponding to fresh biomass and urban emissions from the Southern California region. In contrast, we observed the highest values of CT_{BC} and f_{BC} for L8 and L9, when synoptic winds were blowing aged biomass burning aerosols along the coast of California from the Camp Fire (Northern California) plume. We estimate that source-to-receptor transport from the Camp Fire to Catalina Island is approximately one week. In comparison, all characteristic timescales for L4-L7 were less than 24 hours. Based on these observations, we can make a conservative statement that rBC-containing particles that are aged less than one day in the Los

https://doi.org/10.5194/acp-2019-769
Preprint. Discussion started: 7 October 2019


Atmospheric Chemistry and Physics Discussions

Angeles basin (either from biomass burning or urban emissions) are not likely to be thickly coated. This is in contrast to other previous SP2 measurements that have been made in other regions, which have suggested that timescales of less than one day are sufficient to thickly coat rBC-containing particles (Moteki and Kondo, 2007; Akagi et al., 2012; Baumgardner et al., 2007; Cheng et al., 2018; Dahlkötter et al., 2014; Kondo et al., 2011; Laborde et al., 2013; Metcalf et al., 2012; Pan et al., 2017; Perring et al., 2017; Schwarz et al., 2008; Shiraiwa et al., 2007; Wang et al., 2014, 2018). However, results reported here are consistent with a recent study by Krasowsky et al. (2018) in the Los Angeles basin that also suggests that rBC-containing particles in the Los Angeles region are not significantly coated within timescales less than one day. Our findings add to a growing body of evidence that suggests that regional differences, like atmospheric context and emission sources, play a significant role in the evolution of rBC mixing state, and more specifically, the rate at which rBC-containing particles acquire coatings.

The evolution of rBC mixing state has important implications on accurately assessing the regional climate benefits of black carbon reductions, particularly in California, and also reducing uncertainty in global radiative forcing of BC in climate models. Understanding the time scales for rBC-containing particles to acquire coatings in different regions is important for accurately quantifying the enhancement of BC light absorption, and also for determining BC lifetime in the atmosphere since hygroscopic coating material can enhance the particle's susceptibility to wet deposition (Zhang et al., 2015). These results emphasize the need for more future field measurements of rBC mixing state in various regions around the world, in order to understand its spatial and temporal differences, and consequently its effect on climate forcing on both a regional and global scale.

4 Conclusion

This study investigates the concentration, size distribution, and mixing state of rBC on Catalina Island (~70 km southwest of Los Angeles) using a single-particle soot photometer (SP2). Measurements were taken during three separate campaigns with varying meteorological conditions and emission sources, in September 2017, December 2017, and November 2018. During the first campaign (7 to 14 September 2017), westerly winds dominated and thus the sampling location was upwind of the dominant regional sources of BC (i.e., urban emissions from the Los Angeles basin). The measurements from the first campaign were largely characteristic of ambient background levels of rBC over the Pacific Ocean, away from the broader urban Los Angeles plume. During the second and third campaigns (20 to 22 December 2017, 12 to 18 November 2018), atypical Santa Ana wind conditions caused measured rBC to include important contributions from large wildfires in California and urban emission from the Los Angeles basin. Furthermore, during the third campaign, rBC from the Camp Fire in Northern California was measured, allowing us to compare the mixing state of aged particles (from Camp Fire) to fresh particles (from Southern California fires and urban Los Angeles emissions).

https://doi.org/10.5194/acp-2019-769
Preprint. Discussion started: 7 October 2019


Atmospheric Chemistry and Physics Discussions

For the first campaign (September 2017), rBC concentrations remained relatively constant throughout the sampling period, and the mean concentration (0.04 μg m^{-3}) was about an order of magnitude lower than previous ground-based measurements of rBC concentrations in the Los Angeles basin (~0.14 μg m^{-3}) (Krasowsky et al., 2016). The mean number fraction of thickly-coated rBC particles (f_{BC}) was 0.27 for this period, slightly lower than the lower end of f_{BC} calculated from flight-based measurements (Metcalf et al., 2012) and slightly higher than the upper end of f_{BC} calculated from ground-based measurements (Krasowsky et al., 2016), all in the Los Angeles basin. The background, ambient population of rBC-containing aerosols off the coast of Los Angeles was characterized by a median coating thickness (CT_{BC}) of ~36 nm. Measurements from this period show that rBC-containing particles over the Pacific Ocean are well-aged, based on the mean f_{BC} and CT_{BC} values.

In contrast, the measurements from the second and third campaigns (December 2017, November 2018) had much larger variability in meteorological conditions and BC sources, compared to the first campaign (September 2017). The Santa Ana wind conditions (northerly to easterly winds), along with large wildfire events across California, directly influenced which BC sources contributed to our measurements. During the second campaign, we measured rBC from urban emissions and wildfires in Southern California (Thomas Fire). In addition to urban and wildfire emissions from Southern California, rBC from Northern California (Camp Fire) was measured during the third campaign. The wide variety of meteorological conditions and BC sources resulted in a wide range of rBC concentrations (~0 to 0.6 μg m^{-3} for the second campaign and ~0 to 1.5 μg m^{-3} for the third campaign) and hourly-averaged f_{BC} (~0 to 0.14 for second campaign, ~0.02 to 0.48 for third campaign).

Using the lag-time method and the LEO method we show that rBC mixing state is highly variable, dependent on emission source and atmospheric aging. Based on source-to-receptor timescales approximated with HYSPLIT back-trajectories, MODIS imagery, and meteorological data, we examine the relationship between atmospheric aging and mixing state. Notably, we find that fresh emissions (biomass burning and urban emissions) from the Southern California region with source-to-receptor timescales of less than a day are not significantly coated, with median CT_{BC} ranging from 5.6 to 13.4 nm. In contrast, we observe elevated f_{BC} (~0.23 to 0.47) and much higher median CT_{BC} (40.7 to 68.6 nm) during periods of known impact from a long-range emission source (Camp Fire in Northern California). Previous studies have concluded that rBC acquire significant coating within hours after emission from the source, but our results suggest that rBC in the Los Angeles area do not get coated as quickly when emissions are blown towards the ocean during Santa Ana wind conditions. Additionally, we observe a modest positive correlation (R^2 = 0.36) between median CT_{BC} and median rBC core diameter, which supports previous suggestions that rBC cores can coagulate as they age in the atmosphere (Laborde et al., 2013; Shiraiwa et al., 2008). We also observed larger median mass diameters for periods where biomass burning emissions were suspected to be the dominant source of rBC, confirming measurements reported in previous studies.

https://doi.org/10.5194/acp-2019-769
Preprint. Discussion started: 7 October 2019

575

Our study, in conjunction with previous studies, confirms that rBC mixing state is highly influenced by atmospheric context (i.e., meteorology, chemical composition of regional atmosphere, and emission sources), which varies widely both spatially and temporally. More field campaigns are needed in a variety of sampling locations with different source contributions and atmospheric contexts to further reduce uncertainty associated with rBC mixing state and its influence on BC atmospheric
580 lifetime, spatial distributions, and radiative forcing. Further measurements can serve as an indicator for how accurately models represent BC mixing state and also improve our understanding of BC global distributions, ultimately reducing uncertainties in BC radiative forcing predicted by climate models. Given that there are less than 20 studies that quantify CT_{BC} using the LEO method, this study confirms that further measurements are necessary in order to narrow the quantitative bounds of rBC mixing state in our climate system, particularly since it has important implications on BC absorption
585 enhancement and atmospheric lifetime.

Data availability

Processed data is available at the following Harvard Dataverse repository:
https://dataverse.harvard.edu/dataverse/catalina_rbc_2017_2018.

590 DOI citations to individual datasets:
Ko, Joseph, 2019, "Time Series Data for Catalina Island rBC Measurements 2017-2018",
https://doi.org/10.7910/DVN/UJAGHY, Harvard Dataverse, V1

Ko, Joseph, 2019, "rBC Coating Thickness from Catalina Island rBC Measurements 2017-2018",
595 https://doi.org/10.7910/DVN/AAYMHH, Harvard Dataverse, V2

Ko, Joseph, 2019, "rBC Size Distribution from Catalina Island rBC Measurements 2017-2018",
https://doi.org/10.7910/DVN/CIMVS4, Harvard Dataverse, V1

600 Due to the extremely large file sizes for the raw SP2 data, they are not publicly available but may be available upon request to the corresponding author.

Video supplement

[DOI link to video supplement will be inserted once approved by TIB AV portal]

Supplement

605 [DOI link will be inserted once supplied by ACP]

https://doi.org/10.5194/acp-2019-769
Preprint. Discussion started: 7 October 2019

Atmospheric Chemistry and Physics Discussions

Competing interests: The authors declare no competing interests.

Acknowledgements

This research was supported by the National Science Foundation under CAREER grant CBET-1752522.

We acknowledge the use of data from the European Centre for Medium-Range Weather Forecasts (ECMWF). Neither the European Commission nor ECMWF is responsible for any use that may be made of the information it contains.

We acknowledge the NOAA Air Resources Laboratory (ARL) for the provision of the HYSPLIT transport and dispersion model and/or READY website (http://www.ready.noaa.gov) used in this publication.

We acknowledge the use of imagery from the NASA Worldview application (https://worldview.earthdata.nasa.gov/), part of the NASA Earth Observing System Data and Information System (EOSDIS).

References

Akagi, S. K., Craven, J. S., Taylor, J. W., McMeeking, G. R., Yokelson, R. J., Burling, I. R., Urbanski, S. P., Wold, C. E., Seinfeld, J. H., Coe, H., Alvarado, M. J. and Weise, D. R.: Evolution of trace gases and particles emitted by a chaparral fire in California, Atmos. Chem. Phys., 12(3), 1397–1421, doi:10.5194/acp-12-1397-2012, 2012.

Baumgardner, D., Kok, G. L. and Raga, G. B.: On the diurnal variability of particle properties related to light absorbing carbon in Mexico City, Atmos. Chem. Phys., 7(10), 2517–2526, doi:10.5194/acp-7-2517-2007, 2007.

Beccario, C.: earth.nullschool.net, last access: 26 August 2019.

Bond, T. C. and Bergstrom, R. W.: Light absorption by carbonaceous particles: An investigative review, Aerosol Sci. Technol., 40(1), 27–67, doi:10.1080/02786820500421521, 2006.

Bond, T. C., Doherty, S. J., Fahey, D. W., Forster, P. M., Berntsen, T., Deangelo, B. J., Flanner, M. G., Ghan, S., Kärcher, B., Koch, D., Kinne, S., Kondo, Y., Quinn, P. K., Sarofim, M. C., Schultz, M. G., Schulz, M., Venkataraman, C., Zhang, H., Zhang, S., Bellouin, N., Guttikunda, S. K., Hopke, P. K., Jacobson, M. Z., Kaiser, J. W., Klimont, Z., Lohmann, U.,

https://doi.org/10.5194/acp-2019-769
Preprint. Discussion started: 7 October 2019

Schwarz, J. P., Shindell, D., Storelvmo, T., Warren, S. G. and Zender, C. S.: Bounding the role of black carbon in the climate system: A scientific assessment, J. Geophys. Res. Atmos., 118(11), 5380–5552, doi:10.1002/jgrd.50171, 2013.

CBS Los Angeles: Danielle Gersh's Weather Forecast (Dec. 20), https://youtu.be/p8dEJ-qoPwA, last access: 26 August 2019, 2017a.

CBS Los Angeles: Evelyn Taft's Weather Forecast (Dec. 20), https://youtu.be/gDH73gLbGDk, last access: 26 August 2019, 2017b.

CBS Los Angeles: Danielle Gersh's Weather Forecast (Dec. 21), https://youtu.be/j_0P09YZuKc, last access: 26 August 2019, 2017c.

CBS Los Angeles: Garth Kemp's Weather Forecast (Dec. 21), https://youtu.be/vpv65O1MP0A, last access: 26 August 2019, 2017d.

CBS Los Angeles: Evelyn Taft's Weather Forecast (Dec. 22), https://youtu.be/I7KkZiduQq4, last access: 26 August 2019, 2017e.

CBS Los Angeles: Markina Brown's Weather Forecast (Dec. 22), https://youtu.be/N7htXoFLVcw, last access: 26 August 2019, 2017f.

Cappa, C. D., Onasch, T. B., Massoli, P., Worsnop, D. R., Bates, T. S., Cross, E. S., Davidovits, P., Hakala, J., Hayden, K. L., Jobson, B. T., Kolesar, K. R., Lack, D. A., Lerner, B. M., Li, S. M., Mellon, D., Nuaaman, I., Olfert, J. S., Petäjä, T., Quinn, P. K., Song, C., Subramanian, R., Williams, E. J. and Zaveri, R. A.: Radiative absorption enhancements due to the mixing state of atmospheric black carbon, Science (80-.)., 337(6098), 1078–1081, doi:10.1126/science.1223447, 2012.

Cheng, Y., Li, S. M., Gordon, M. and Liu, P.: Size distribution and coating thickness of black carbon from the Canadian oil sands operations, Atmos. Chem. Phys., 18(4), 2653–2667, doi:10.5194/acp-18-2653-2018, 2018.

Dahlkötter, F., Gysel, M., Sauer, D., Minikin, A., Baumann, R., Seifert, P., Ansmann, A., Fromm, M., Voigt, C. and Weinzierl, B.: The Pagami Creek smoke plume after long-range transport to the upper troposphere over Europe – Aerosol properties and black carbon mixing state, Atmos. Chem. Phys., 14(12), 6111–6137, doi:10.5194/acp-14-6111-2014, 2014.

https://doi.org/10.5194/acp-2019-769
Preprint. Discussion started: 7 October 2019

Gao, R. S., Schwarz, J. P., Kelly, K. K., Fahey, D. W., Watts, L. A., Thompson, T. L., Spackman, J. R., Slowik, J. G., Cross, E. S., Han, J. H., Davidovits, P., Onasch, T. B. and Worsnop, D. R.: A novel method for estimating light-scattering properties of soot aerosols using a modified single-particle soot photometer, Aerosol Sci. Technol., 41(2), 125–135, doi:10.1080/02786820601118398, 2007.

He, C., Liou, K. N., Takano, Y., Zhang, R., Levy Zamora, M., Yang, P., Li, Q. and Leung, L. R.: Variation of the radiative properties during black carbon aging: Theoretical and experimental intercomparison, Atmos. Chem. Phys., 15(20), doi:10.5194/acp-15-11967-2015, 2015.

Hughes, L. S., Allen, J. O., Bhave, P., Kleeman, M. J., Cass, G. R., Liu, D. Y., Fergenson, D. P., Morrical, B. D. and Prather, K. A.: Evolution of atmospheric particles along trajectories crossing the Los Angeles basin, Environ. Sci. Technol., 34(15), 3058–3068, doi:10.1021/es9908671, 2000.

IPCC: Climate Change 2013: The Physical Science Basis. Contribution of Working Group I to the Fifth Assessment Report of the Intergovernmental Panel on Climate Change, Cambridge University Press, Cambridge, United Kingdom and New York, NY, USA, https://doi.org/10.1017/CBO9781107415324, 2013.

Jaross, G.: OMPS-NPP L2 NM Ozone (O3) Total Column swath orbital V2, Greenbelt, MD, USA, Goddard Earth Sciences Data and Information Services Center (GES DISC), last access: 26 August 2019, doi:10.5067/0WF4HAAZ0VHK, 2017.

Johnson, G. R., Ristovski, Z. D., D'Anna, B. and Morawska, L.: Hygroscopic behavior of partially volatilized coastal marine aerosols using the volatilization and humidification tandem differential mobility analyzer technique, J. Geophys. Res. D Atmos., 110(20), 1–14, doi:10.1029/2004JD005657, 2005.

Justice, C. O., Giglio, L., Korontzi, S., Owens, J., Morisette, J., Roy, D., Descloitres, J., Alleaume, S., Petitcolin, F. and Kaufman, Y. J.: The MODIS fire products. Remote Sensing of Environment 83:244-262. doi:10.1016/S0034-4257(02)00076-7, 2002.

Knox, A., Evans, G. J., Brook, J. R., Yao, X., Jeong, C. H., Godri, K. J., Sabaliauskas, K. and Slowik, J. G.: Mass absorption cross-section of ambient black carbon aerosol in relation to chemical age, Aerosol Sci. Technol., 43(6), 522–532, doi:10.1080/02786820902777207, 2009.

Kondo, Y., Matsui, H., Moteki, N., Sahu, L., Takegawa, N., Kajino, M., Zhao, Y., Cubison, M. J., Jimenez, J. L., Vay, S., Diskin, G. S., Anderson, B., Wisthaler, A., Mikoviny, T., Fuelberg, H. E., Blake, D. R., Huey, G., Weinheimer, A. J., Knapp,

https://doi.org/10.5194/acp-2019-769
Preprint. Discussion started: 7 October 2019

D. J. and Brune, W. H.: Emissions of black carbon, organic, and inorganic aerosols from biomass burning in North America and Asia in 2008, J. Geophys. Res. Atmos., 116(8), 1–25, doi:10.1029/2010JD015152, 2011.

Krasowsky, T. S., McMeeking, G. R., Wang, D., Sioutas, C. and Ban-Weiss, G. A.: Measurements of the impact of atmospheric aging on physical and optical properties of ambient black carbon particles in Los Angeles, Atmos. Environ., 142, 496–504, doi:10.1016/j.atmosenv.2016.08.010, 2016.

Krasowsky, T. S., Mcmeeking, G. R., Sioutas, C. and Ban-Weiss, G.: Characterizing the evolution of physical properties and mixing state of black carbon particles: From near a major highway to the broader urban plume in Los Angeles, Atmos. Chem. Phys., 18(16), 11991–12010, doi:10.5194/acp-18-11991-2018, 2018.

Laborde, M., Mertes, P., Zieger, P., Dommen, J., Baltensperger, U. and Gysel, M.: Sensitivity of the Single Particle Soot Photometer to different black carbon types, Atmos. Meas. Tech., 5(5), 1031–1043, doi:10.5194/amt-5-1031-2012, 2012.

Laborde, M., Crippa, M., Tritscher, T., Jurányi, Z., Decarlo, P. F., Temime-Roussel, B., Marchand, N., Eckhardt, S., Stohl, A., Baltensperger, U., Prévôt, A. S. H., Weingartner, E. and Gysel, M.: Black carbon physical properties and mixing state in the European megacity Paris, Atmos. Chem. Phys., 13(11), 5831–5856, doi:10.5194/acp-13-5831-2013, 2013.

Liu, D., Allan, J. D., Young, D. E., Coe, H., Beddows, D., Fleming, Z. L., Flynn, M. J., Gallagher, M. W., Harrison, R. M., Lee, J., Prevot, A. S. H., Taylor, J. W., Yin, J., Williams, P. I. and Zotter, P.: Size distribution, mixing state and source apportionment of black carbon aerosol in London during winter time, Atmos. Chem. Phys., 14(18), 10061–10084, doi:10.5194/acp-14-10061-2014, 2014.

McMeeking, G. R., Good, N., Petters, M. D., McFiggans, G. and Coe, H.: Influences on the fraction of hydrophobic and hydrophilic black carbon in the atmosphere, Atmos. Chem. Phys., 11(10), 5099–5112, doi:10.5194/acp-11-5099-2011, 2011.

Metcalf, A. R., Craven, J. S., Ensberg, J. J., Brioude, J., Angevine, W., Sorooshian, A., Duong, H. T., Jonsson, H. H., Flagan, R. C. and Seinfeld, J. H.: Black carbon aerosol over the Los Angeles Basin during CalNex, J. Geophys. Res. Atmos., 117(8), 1–24, doi:10.1029/2011JD017255, 2012.

Moteki, N., Kondo, Y., Miyazaki, Y., Takegawa, N., Komazaki, Y., Kurata, G., Shirai, T., Blake, D. R., Miyakawa, T. and Koike, M.: Evolution of mixing state of black carbon particles: Aircraft measurements over the western Pacific in March 2004, Geophys. Res. Lett., 34(11), doi:10.1029/2006GL028943, 2007.

https://doi.org/10.5194/acp-2019-769
Preprint. Discussion started: 7 October 2019

Moteki, N., Kondo, Y., Oshima, N., Takegawa, N., Koike, M., Kita, K., Matsui, H. and Kajino, M.: Size dependence of wet removal of black carbon aerosols during transport from the boundary layer to the free troposphere, Geophys. Res. Lett., 39(13), 2–5, doi:10.1029/2012GL052034, 2012.

Pan, X., Kanaya, Y., Taketani, F., Miyakawa, T., Inomata, S., Komazaki, Y., Tanimoto, H., Wang, Z., Uno, I. and Wang, Z.: Emission characteristics of refractory black carbon aerosols from fresh biomass burning: A perspective from laboratory experiments, Atmos. Chem. Phys., 17(21), 13001–13016, doi:10.5194/acp-17-13001-2017, 2017.

Ramanathan, V. and Carmichael, G.: Global and regional climate changes due to black carbon, Nat. Geosci., 1(4), 221–227, doi:10.1038/ngeo156, 2008.

Perring, A. E., Schwarz, J. P., Markovic, M. Z., Fahey, D. W., Jimenez, J. L., Campuzano-Jost, P., Palm, B. D., Wisthaler, A., Mikoviny, T., Diskin, G., Sachse, G., Ziemba, L., Anderson, B., Shingler, T., Crosbie, E., Sorooshian, A., Yokelson, R. and Gao, R. S.: In situ measurements of water uptake by black carbon-containing aerosol in wildfire plumes, J. Geophys. Res., 122(2), doi:10.1002/2016JD025688, 2017.

Sahu, L. K., Kondo, Y., Moteki, N., Takegawa, N., Zhao, Y., Cubison, M. J., Jimenez, J. L., Vay, S., Diskin, G. S., Wisthaler, A., Mikoviny, T., Huey, L. G., Weinheimer, A. J. and Knapp, D. J.: Emission characteristics of black carbon in anthropogenic and biomass burning plumes over California during ARCTAS-CARB 2008, J. Geophys. Res. Atmos., 117(16), 1–20, doi:10.1029/2011JD017401, 2012.

Schwarz, J. P., Gao, R. S., Fahey, D. W., Thomson, D. S., Watts, L. A., Wilson, J. C., Reeves, J. M., Darbeheshti, M., Baumgardner, D. G., Kok, G. L., Chung, S. H., Schulz, M., Hendricks, J., Lauer, A., Kärcher, B., Slowik, J. G., Rosenlof, K. H., Thompson, T. L., Langford, A. O., Loewenstein, M. and Aikin, K. C.: Single-particle measurements of midlatitude black carbon and light-scattering aerosols from the boundary layer to the lower stratosphere, J. Geophys. Res. Atmos., 111(16), doi:10.1029/2006JD007076, 2006.

Schwarz, J. P., Gao, R. S., Spackman, J. R., Watts, L. A., Thomson, D. S., Fahey, D. W., Ryerson, T. B., Peischl, J., Holloway, J. S., Trainer, M., Frost, G. J., Baynard, T., Lack, D. A., de Gouw, J. A., Warneke, C. and Del Negro, L. A.: Measurement of the mixing state, mass, and optical size of individual black carbon particles in urban and biomass burning emissions, Geophys. Res. Lett., 35(13), 1–5, doi:10.1029/2008GL033968, 2008.

Schroeder, W., Oliva, P., Giglio, L., & Csiszar, I. A.: The New VIIRS 375 m active fire detection data product: algorithm description and initial assessment. Remote Sensing of Environment, 143, 85-96. doi:10.1016/j.rse.2013.12.008, 2014.

https://doi.org/10.5194/acp-2019-769
Preprint. Discussion started: 7 October 2019

Shiraiwa, M., Kondo, Y., Moteki, N., Takegawa, N., Miyazaki, Y. and Blake, D. R.: Evolution of mixing state of black carbon in polluted air from Tokyo, Geophys. Res. Lett., 34(16), 2–6, doi:10.1029/2007GL029819, 2007.

Shiraiwa, M., Kondo, Y., Moteki, N., Takegawa, N., Sahu, L. K., Takami, A., Hatakeyama, S., Yonemura, S. and Blake, D. R.: Radiative impact of mixing state of black carbon aerosol in Asian outflow, J. Geophys. Res. Atmos., 113(24), 1–13, doi:10.1029/2008JD010546, 2008.

Slowik, J. G., Cross, E. S., Han, J. H., Davidovits, P., Onasch, T. B., Jayne, J. T., Williams, L. R., Canagaratna, M. R., Worsnop, D. R., Chakrabarty, R. K., Moosmüller, H., Arnott, W. P., Schwarz, J. P., Gao, R. S., Fahey, D. W., Kok, G. L. and Petzold, A.: An Inter-Comparison of Instruments Measuring Black Carbon Content of Soot Particles, Aerosol Sci. Technol., 41(3), 295–314, doi:10.1080/02786820701197078, 2007.

Stein, A. F., Draxler, R. R., Rolph, G. D., Stunder, B. J. B., Cohen, M. D. and Ngan, F.: Noaa's hysplit atmospheric transport and dispersion modeling system, Bull. Am. Meteorol. Soc., 96(12), 2059–2077, doi:10.1175/BAMS-D-14-00110.1, 2015.

Stephens, M., Turner, N. and Sandberg, J.: Particle identification by laser-induced incandescence in a solid-state laser cavity, Appl. Opt., 42(19), 3726, doi:10.1364/ao.42.003726, 2003.

Todey, D. P., Herzmann, D. E., and Takle, G. S.: The Iowa Environmental Mesonet – combining networks into a single network, Preprints 6th Symposium on Integrated Observing Systems, Annual Meeting of the American Meteorological Society, 14–17 January 2002, Orlando, FL, USA, 2002

Torres, O.: OMI/Aura Near UV Aerosol Optical Depth and Single Scattering Albedo 1-orbit L2 Swath 13x24 km V003, Greenbelt, MD, USA, Goddard Earth Sciences Data and Information Services Center (GES DISC), last access: 26 August 2019, 10.5067/Aura/OMI/DATA2004, 2006.

Wang, Q., Huang, R. J., Cao, J., Han, Y., Wang, G., Li, G., Wang, Y., Dai, W., Zhang, R. and Zhou, Y.: Mixing state of black carbon aerosol in a heavily polluted urban area of China: Implications for light absorption enhancement, Aerosol Sci. Technol., 48(7), 689–697, doi:10.1080/02786826.2014.917758, 2014.

Wang, Q., Cao, J., Han, Y., Tian, J., Zhang, Y., Pongpiachan, S., Zhang, Y., Li, L., Niu, X., Shen, Z., Zhao, Z., Tipmanee, D., Bunsomboonsakul, S., Chen, Y. and Sun, J.: Enhanced light absorption due to the mixing state of black carbon in fresh biomass burning emissions, Atmos. Environ., 180(December 2017), 184–191, doi:10.1016/j.atmosenv.2018.02.049, 2018.

https://doi.org/10.5194/acp-2019-769
Preprint. Discussion started: 7 October 2019

Atmospheric Chemistry and Physics Discussions

805 World Health Organization (WHO): Health effects of black carbon, ISBN: 9789289002653, available at: http://www.euro.who.int/__data/assets/pdf_file/0004/162535/e96541.pdf, last access: 26 August 2019, 2012.

Zhang, J., Liu, J., Tao, S. and Ban-Weiss, G. A.: Long-range transport of black carbon to the Pacific Ocean and its dependence on aging timescale, Atmos. Chem. Phys., 15(20), 11521–11535, doi:10.5194/acp-15-11521-2015, 2015.